Inorganic Chemistry

Article

pubs.acs.org/IC

Ferrocene-Decorated (Phthalocyaninato)(Porphyrinato) Double- and Triple-Decker Rare Earth Complexes: Synthesis, Structure, and Electrochemical Properties

Peihua Zhu,[†] Xiuwen Zhang,[§] Hailong Wang,[‡] Yuexing Zhang,[‡] Yongzhong Bian,*[,‡] and Jianzhuang Jiang*[,‡,§]

[†]Contribution from School of Chemistry and Chemical Engineering, University of Jinan, Jinan 250022, China

[‡]Department of Chemistry, University of Science and Technology Beijing, Beijing 100083, China

[§]Department of Chemistry, Shandong University, Jinan 250100, China

Supporting Information

ABSTRACT: A series of four mixed (phthalocyaninato)(porphyrinato) rare earth double-decker complexes (*Pc*)M[Por(Fc)$_2$] [*Pc* = phthalocyaninate; Por(Fc)$_2$ = 5,15-di(ferrocenyl)porphyrinate; M = Eu (**1**), Y (**2**), Ho (**3**), Lu (**4**)] and their europium(III) triple-decker counterpart (*Pc*)Eu(*Pc*)Eu[Por(Fc)$_2$] (**5**), each with two ferrocenyl units at the *meso*-positions of their porphyrin ligands, have been designed and prepared. The double- and triple-decker complexes **1**−**5** were characterized by elemental analysis and various spectroscopic methods. The molecular structures of two double-deckers **1** and **4** were also determined by single-crystal X-ray diffraction analysis. Electrochemical studies of these novel sandwich complexes revealed two consecutive ferrocene-based one-electron oxidation waves, suggesting the effective electronic coupling between the two ferrocenyl units. Nevertheless, the separation between the two consecutive ferrocene-based oxidation waves increases from **1** to **4**, along with the decrease of rare earth ionic radius, indicating the effect of rare earth size on tuning the coupling between the two ferrocenyl units. Furthermore, the splitting between the two ferrocene-based one-electron oxidations for triple-decker **5** is even smaller than that for **1**, showing that the electronic interaction between the two ferrocene centers can also be tuned through changing the linking sandwich framework from double-decker to triple-decker. For further understanding of the electronic coupling between ferrocenyl groups, DFT calculation is carried out to clarify the electronic delocalization and the molecular orbital distribution in these double-decker complexes.

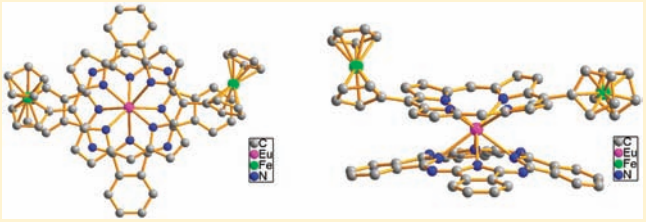

INTRODUCTION

Covalently linked arrays of photo- and redox-active units with long-range electronic coupling behavior have aroused increasing interest for their potential applications in molecular electronics.[1,2] Owing to its well-defined electrochemistry, ferrocene has been extensively utilized in the construction of such multicomponent systems for the purpose of detecting and investigating the metal−metal coupling by means of spectroscopic analyses and electrochemical methods.[3] Among various frameworks linking the ferrocenyl units, porphyrins[4] and their artificial analogues, phthalocyanines,[5] are very attractive because of their unique cyclic π-conjugated tetrapyrrole structures and redox and photophysical properties. However, despite quite a large number of reports on the di- and multiferrocenyl-appended porphyrin[6] and phthalocyanine architectures,[7] examples exhibiting strong electronic coupling between the ferrocenyl units connected via tetrapyrrole framework remain rare due to their large distance and, in particular, unsuitable relative orientation associated with the free rotation of these ferrocenyl units. Boyd et al.[8] and Rhee et al.[8b] reported 5,15-bis(ferrocenyl)-β-octaalkyl-porphyrins with *syn*-conformation, which have shown long-range metal−metal coupling between the two *meso*-ferrocenyl units. Augel et al. found that 5,15-diferrocenyl-10-phenylporphyrin[8c] and both *cis*- and *trans*-isomers of *meso*-substituted diferrocenyldipentafluorophenyl porphyrins[8d] formed mixed valence states in given electrochemistry conditions. Recently, Nemykin and co-workers systematically investigated the long-range electronic communication for a series of *meso*-substituted bis-, tris-, and tetraferrocenyl porphyrins.[8e−j] Their results suggest that the steric hindrance induced stable *syn*-conformation of *meso*-ferrocenyl units relative to the porphyrin core is not the only access to the strong electronic coupling.

However, tetrapyrrole derivatives such as porphyrins and phthalocyanines, containing four pyrrole or isoindole nitrogen atoms, are able to coordinate with rare earth metals, forming sandwich-type complexes in the form of double- and triple-decker.[9] Because of the intramolecular π−π interactions and the intrinsic nature of the rare earth metal centers, these novel complexes display characteristic features that cannot be found in their nonsandwich counterparts, enabling them to be used

Received: December 5, 2011
Published: May 3, 2012

Scheme 1. Synthesis of Metal Free Porphyrin $H_2Por(Fc)_2$ and Double- and Triple-Decker Complexes 1−5

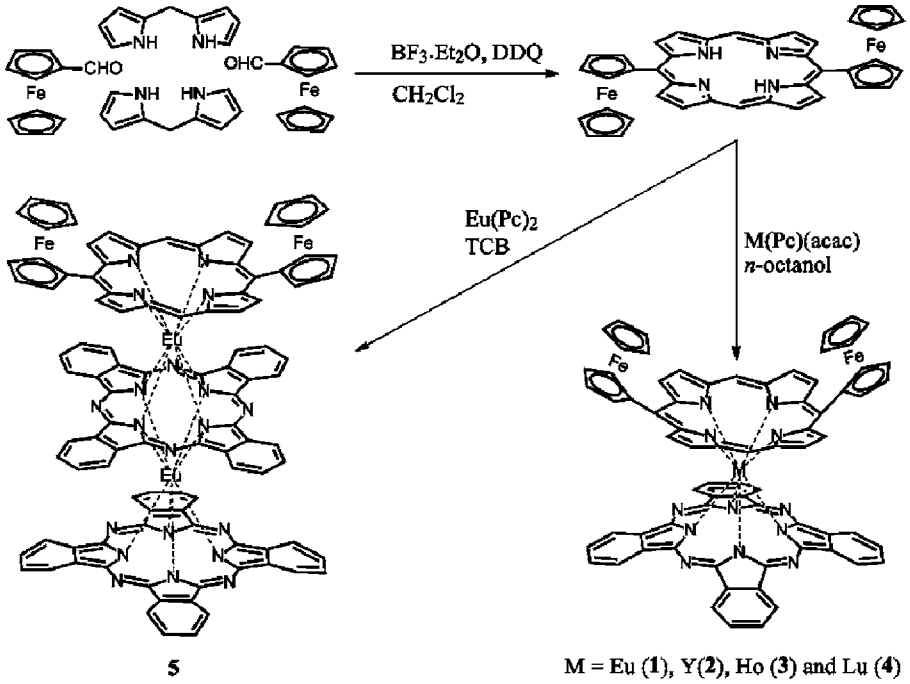

in different areas such as field effect transistors,[10] molecular magnets,[11] and molecular-based multibit information storage devices.[12] In particular, both the two tetraprryole ligands in the double-decker as well as the outer two ligands in the triple-decker molecule are revealed to adopt a domed conformation toward the central rare earth ion(s).[9] This renders it possible to tune the substituents like the phenyl groups attached at the *meso*-positions of the porphyrin ligand in a *syn*-configuration with respect to the porphyrin ring due to their restricted rotation associated with the steric hindrance from the *Pc* ring in the mixed (phthalocyaninato)(porphyrinato) rare earth sandwich complexes.[13] As a result, we designed and prepared a series of tetrapyrrole−ferrocene conjugates in which two bulky ferrocenyl units are linked with (phthalocyaninato)(porphyrinato) double- or triple-decker framework, namely, $M(Pc)[Por(Fc)_2]$ [M = Eu (**1**), Y (**2**), Ho (**3**), Lu (**4**)] and $Eu_2(Pc)_2[Por(Fc)_2]$ (**5**). Electrochemical studies clearly reveal the effective electronic coupling between the two ferrocenyl units attached at the *meso*-positions of the porphyrin ring due to their suitable orientation and distance adjusted by the sandwich structure of tetrapyrrole rare earth complexes. Nevertheless, the interaction between the two ferrocene centers has been revealed easily tunable through changing either the rare earth metal or the linking sandwich framework because of the dependence of the tetrapyrrole doming degree in sandwich molecules on the rare earth size and sandwich form.[14] This gives a useful hint on developing novel molecular systems containing multiple photoactive and redox-active centers with long-range electronic coupling for applications in molecular electronics.

RESULTS AND DISCUSSION

Synthesis and Spectroscopic Characterization. Metal free porphyrin with two ferrocenyl units attached at the two opposite *meso*-positions, $H_2Por(Fc)_2$, was prepared by a condensation reaction between ferrocene aldehyde and dipyrrolemethane.[15] Treatment of $H_2Por(Fc)_2$ with the half-sandwich complexes $M^{III}(acac)(Pc)$ (M = Eu, Y, Ho, Lu), which were generated in situ from corresponding $M(acac)_3{\cdot}nH_2O$ (M = Eu, Y, Ho, Lu) and phthalonitrile in the presence of 1,8-diazabicyclo[5.4.0]-undec-7-ene (DBU), in refluxing *n*-octanol led to the formation of mixed (phthalocyaninato)(porphyrianto) rare earth double-deckers $M(Pc)[Por(Fc)_2]$ [M = Eu (**1**), Y (**2**), Ho (**3**), Lu (**4**)] in the yields of 5−20%, Scheme 1. The yields of the series of double-deckers **1**−**4**, which show dependence on the rare earth ionic size, diminish gradually along with the lanthanide contraction as a result of an increase in axial compression between the two tetrapyrrole macrocyclic ligands. The mixed ring europium triple-decker $Eu_2(Pc)_2[Por(Fc)_2]$ (**5**) was obtained from the reaction of metal free porphyrin $H_2Por(Fc)_2$ with $Eu(Pc)_2$ in the presence of $Eu(acac)_3{\cdot}H_2O$, Scheme 1. As expected, decreased axial compression between two neighboring tetrapyrrole ligands associated with increased ring-to-ring separation and decreased $\pi-\pi$ interaction in mixed (phthalocyaninato)(porphyrinato) triple-decker counterpart induces the easy formation of corresponding mixed ring triple-decker complex.[9] This is verified by the isolation of compound **5** in the high yield of 70%.

All these newly prepared mixed ring rare earth complexes were fully characterized with elemental analysis and a range of spectroscopic methods, Table 1. The MALDI-TOF mass spectra of these compounds clearly show intense signals for the molecular ion M^+. The isotopic pattern closely resembled the simulated one as exemplified by the spectrum of the double-decker complex **4** given in Figure 1.

Because of the presence of the unpaired electron and the paramagnetic nature of some of the rare earth ions, the NMR data for these double-decker complexes are difficult to obtain.[9] Upon addition of hydrazine hydrate, which reduces the double-deckers into corresponding monoanions containing no unpaired electron in the HOMO of the double-decker molecules, satisfactory ^1H NMR spectra could be obtained for the double-decker complexes $M(Pc)[Por(Fc)_2]$ [M = Eu (**1**), Y (**2**), Lu (**4**)]. The data together with the assignment are given in Table S1 (Supporting Information). As shown in Figure S1 (Supporting Information) for $Lu(Pc)[Por(Fc)_2]$ (**4**), the signals

dx.doi.org/10.1021/ic202613r | Inorg. Chem. 2012, 51, 5651−5659

Table 1. Analytical and Mass Spectroscopic Data for the Double- and Triple-Deckers 1−5[a]

cmpd	yield (%)	M^+ (m/z)[b]	analysis (%) C	H	N
Eu(*Pc*)[Por(Fc)$_2$] (**1**)	20	1341.2 (1341.2)	60.44 (60.04)[c]	3.38 (3.11)[c]	11.67 (11.51)[c]
Y(*Pc*)[Por(Fc)$_2$] (**2**)	12	1277.5 (1277.2)	62.70 (62.75)[c]	3.32 (3.25)[c]	12.00 (12.03)[c]
Ho(*Pc*)[Por(Fc)$_2$] (**3**)	10	1353.5 (1353.2)	63.90 (63.88)	3.47 (3.28)	12.36 (12.42)
Lu(*Pc*)[Por(Fc)$_2$] (**4**)	5	1363.5 (1363.2)	63.64 (63.41)	3.38 (3.25)	12.41 (12.32)
Eu$_2$(*Pc*)$_2$[Por(Fc)$_2$] (**5**)	70	2006.8 (2006.2)	56.47 (56.73)[d]	2.82 (2.78)[d]	12.53 (12.48)[d]

[a]Calculated values given in parentheses. [b]By MALDI-TOF mass spectrometry. [c]Contains 1 equiv of solvated $CHCl_3$. [d]Contains 2 equiv of solvated $CHCl_3$.

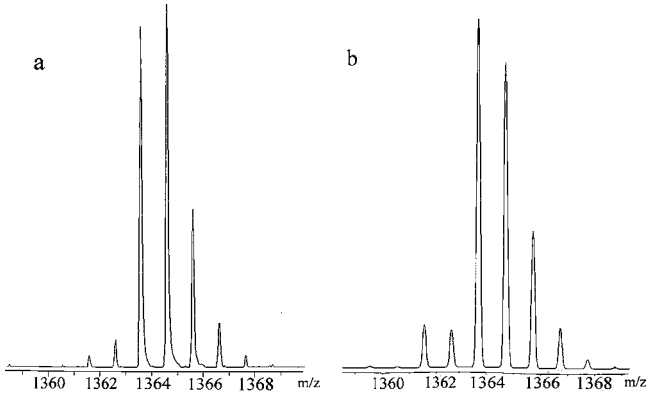

Figure 1. (a) Experimental and (b) simulated isotopic patterns for the molecular ion of Lu(*Pc*)[Por(Fc)$_2$] (**4**) shown in the MALDI-TOF mass spectrum.

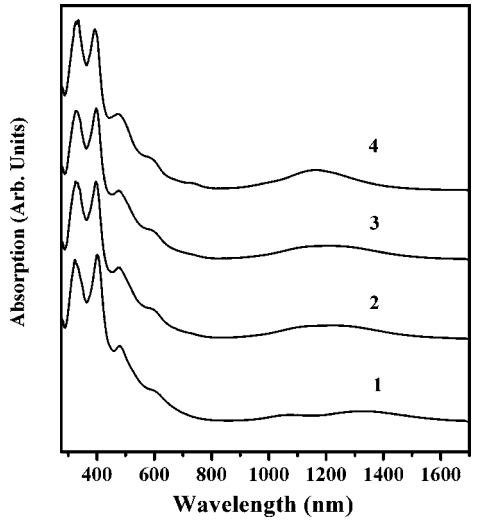

Figure 2. Electronic absorption spectra of Eu(*Pc*)[Por(Fc)$_2$] (**1**), Y(*Pc*)[Por(Fc)$_2$] (**2**), Ho(*Pc*)[Por(Fc)$_2$] (**3**), and Lu(*Pc*)[Por(Fc)$_2$] (**4**) in $CHCl_3$.

at δ 9.13 and 8.83 are attributed to the α protons of the *Pc* ring, while those at δ 8.19 and 7.94 are attributed to the β protons of *Pc* ring. Also as the result of the *trans*-disposition of the ferrocenyl units, the Por β protons are no longer equivalent. The signals for the β protons of Por(Fc)$_2$ are split into two doublets at δ 9.41 and 8.40, respectively. The Por *meso*-protons resonate as a sharp singlet at δ 8.50. The protons of ferrocenyl groups give two signals at δ 4.68 (10H) and 4.60 (8H), respectively. The assignment was unambiguously confirmed by the ^{1}H−^{1}H COSY spectrum, Figure S2 (Supporting Information). The spectrum for the yttrium analogue **2** is similar to that of **4** except the unresolved signal for the ferrocenyl protons at δ 4.66 (18H). In the case of Ho(*Pc*)[Por(Fc)$_2$] (**3**), the ^{1}H NMR spectrum is obscured by the paramagnetic Ho(III) center severely.[16a] However, despite the containing of paramagnetic Eu(III) center, the ^{1}H NMR spectra for double-decker Eu(*Pc*)[Por(Fc)$_2$] (**1**) and its triple-decker analogue Eu$_2$(*Pc*)$_2$[Por(Fc)$_2$] (**5**) are acquired with virtually all of the expected signals, which can be unambiguously assigned after taking the lanthanide-induced shift (LIS) effect of Eu(III) into account,[16] Table S1 (Supporting Information).

The electronic absorption spectra of double- and triple-decker complexes (**1**−**5**) were recorded in $CHCl_3$, and the data are summarized in Table 2. The spectra of **1**−**4** (Figure 2) and **5** (Figure 3) exhibit typical features of (phthalocyaninato)(porphyrinato) double- and triple-decker complexes, respectively.[13] In particular, all the four double-decker absorption spectra show a typical characteristic marker band for single-hole bis(tetrapyrrole) rare earth complexes in the near IR region, 1165−1330 nm, due to the transition from the second HOMO to the semioccupied HOMO orbital.[13b] The fact that this characteristic near IR band shifts to the blue as the size of the metal center decreases indicates the increased π−π interaction between the two tetrapyrrole rings in the double-decker complexes due to the decreased ring-to-ring distance along with the rare earth contraction.[9,13,14]

Structural Studies. The single crystals of double-deckers Eu(*Pc*)[Por(Fc)$_2$] (**1**) and Lu(*Pc*)[Por(Fc)$_2$] (**4**) were grown by slow diffusion of CH_3OH into their $CHCl_3$ solutions. The molecular structures were determined by single-crystal X-ray analysis. Compound **1** crystallizes in the triclinic system, $P\bar{1}$ space group, whereas **4** crystallizes in the monoclinic system, $P2/c$ space group. The two double-deckers have similar molecular structures (Table 3), as exemplified by the molecular

Table 2. Electronic Absorption Data for the Double- and Triple-Deckers 1−5 in $CHCl_3$

cmpd	λ_{max} (nm) (log ε)						
1	326 (4.87)	402 (4.90)	480 (4.56)	602 (4.15)	730 (sh)	1076 (3.76)	1330 (3.89)
2	328 (4.89)	398 (4.89)	476 (4.55)	598 (4.15)	732 (3.59)	1115 (3.89)	1262 (3.91)
3	328 (4.88)	398 (4.89)	476 (4.56)	596 (4.15)	733 (3.60)	1130 (3.90)	1245 (3.90)
4	330 (4.90)	392 (4.88)	472 (4.56)	594 (4.16)	734 (3.65)		1165 (3.99)
5	340 (5.14)	402 (4.78)	535 (4.48)	624 (4.63)	734 (4.38)		

dx.doi.org/10.1021/ic202613r | *Inorg. Chem.* 2012, 51, 5651−5659

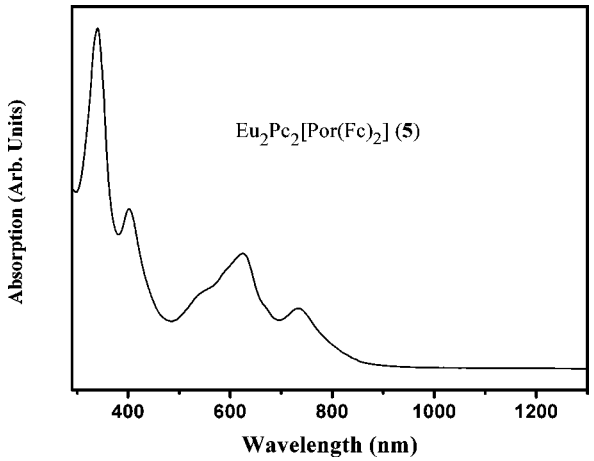

Figure 3. Electronic absorption spectrum of $Eu_2(Pc)_2[Por(Fc)_2]$ (**5**) in $CHCl_3$.

Table 3. Comparison of the Structural Data for 1 and 4

	1	4
average M–N(Por) bond distance (Å)	2.450	2.391
average M–N[*Pc*] bond distance (Å)	2.493	2.423
M–N_4(Por) plane distance (Å)	1.303	1.224
M–N_4(*Pc*) plane distance (Å)	1.510	1.424
interplanar distance (Å)	2.813	2.648
dihedral angle between the two N_4 planes (deg)	1.25	0.97
average dihedral angle φ for the Por ring (deg)[a]	11.84	13.72
average dihedral angle φ for the *Pc* ring (deg)[a]	12.24	17.86
average twist angle θ (deg)[b]	42.15	41.15
distances between two iron atoms (Å)	13.065	13.426
angle between two Fc units (deg)[c]	67.62	42.23
dihedral angle between Cp ring and N4 plan of Por ring (deg)[d]	36.92/77.76	64.90/62.34

[a]The average dihedral angle of the individual isoindole rings with respect to the corresponding N_4 mean plane. [b]Defined as the rotation angle of one ring away from the eclipsed conformation of the two rings. [c]Defined as the dihedral angle between the two Cp rings directly connected to the *meso*-C of Por. [d]Defined as the dihedral angle between the Cp ring directly connected in the *meso*-C of Por and N4 plan of the Por ring.

structure of Eu(*Pc*)[Por(Fc)$_2$] (**1**) in Figure 4. The europium center is coordinated by eight nitrogen atoms from the isoindole and pyrrole of the *Pc* and Por rings, respectively, forming a nearly perfect square antiprism with a ring-to-ring separation of 2.813 Å (as defined by the two N4 mean planes). The metal center lies closer to the N4 plane of Por by 0.207 Å, probably because of the larger cavity of Por. The two N4 planes are virtually parallel (dihedral angle 1.247°), but the two ligands are significantly domed. The average dihedral angle (φ) of the individual isoindole or pyrrole rings with respect to the corresponding N4 mean plane is 11.84° for the Por and 12.24° for the *Pc* ring, respectively. The average M–N bond distances and the interplanar separation decrease with the size of the metal center, while the extent of ligand deformation increases from Eu to Lu (Table 3). The average twist angle, defined as the rotation angle of one ring away from the eclipsed conformation of the two rings, is 42.15° for **1** and 41.15° for **4**, indicating that the two ligands are slightly deflective from the staggered conformation. Particularly, the distance between the two ferrocene iron atoms are 13.065 and 13.426 Å for **1** and **4**, respectively, which are larger than that in the $\alpha,\beta,\alpha,\beta$-5,10,15,20-tetrakis(ferrocenyl)porphyrinate zinc(II) complex with a distance between the α,α- and β,β-ferrocene iron atoms being 11.73 and 11.52 Å, respectively.[6g] A notable difference between the molecular structures of **1** and **4** is the relative orientation of the ferrocene subunits, Figures 4 and S3 (Supporting Information). The torsion angle between the two ferrocene subunits is 67.62° for **1**, which is larger than that for **4** (42.23°). In addition, the dihedral angle between the cyclopentadienyl (Cp) rings directly connected to Por and the N4 plan of the Por ring are 36.92° and 77.76° for **1**, while those for **4** are 64.90° and 62.34°, showing relatively smaller rotational feasibility of the ferrocene subunits in **4** than that in **1**, due mainly to the difference of steric hindrance induced by the different size of Eu and Lu atoms in the double-deckers.

Electrochemical Properties. The electrochemical properties of all the sandwich-type complexes **1**–**5** were studied by cyclic voltammetry (CV) and differential pulse voltammetry (DPV) in CH_2Cl_2. As shown in Figures 5 and S4 (Supporting Information), all the four double-decker compounds M(*Pc*)[Por(Fc)$_2$] [M = Eu (**1**), Y (**2**), Ho (**3**), Lu (**4**)] exhibit three quasi-reversible one-electron oxidations labeled as Oxd_1–Oxd_3 and two quasi-reversible one-electron reductions labeled as Red_1–Red_2 within the electrochemical window of CH_2Cl_2. The half-wave potentials are summarized in Table 4. Comparison with the electrochemical behavior of sandwich analogues M(*Pc*)(TClPP) (M = Y, La–Lu except Ce and Pm)[13b] and that of ferrocenyl-appended monomeric porphyrins[8] clearly reveals the nature of the tetrapyrrole-based processes for the first reduction, second reduction, and third oxidation of these double-decker complexes **1**–**4**. The difference of the redox potentials of Red_1 and Red_2 for M(*Pc*)[Por(Fc)$_2$], $\Delta E^\circ_{1/2}$, which actually corresponds to the potential difference between the first oxidation and first reduction of $\{M(Pc)[Por(Fc)_2]\}^-$, decreases gradually from 1417 mV for Eu(*Pc*)[Por(Fc)$_2$] (**1**) to 1380 mV

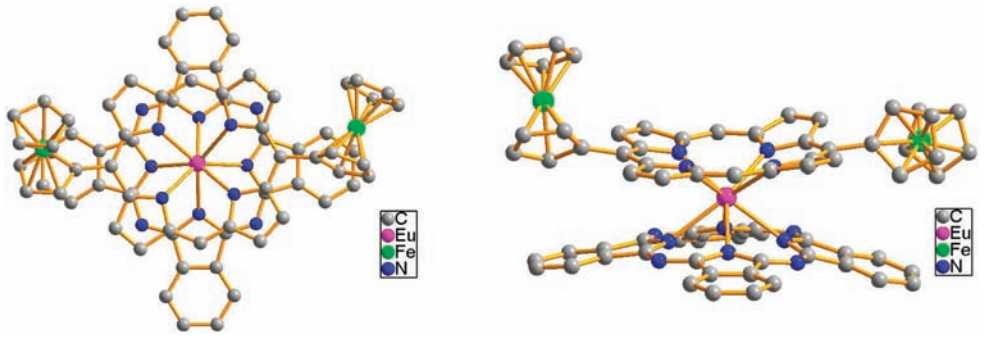

Figure 4. Molecular structure of Eu(*Pc*)[Por(Fc)$_2$] (**1**) from two perspectives with hydrogen atoms and solvent molecules omitted for clarity.

dx.doi.org/10.1021/ic202613r | *Inorg. Chem.* 2012, 51, 5651–5659

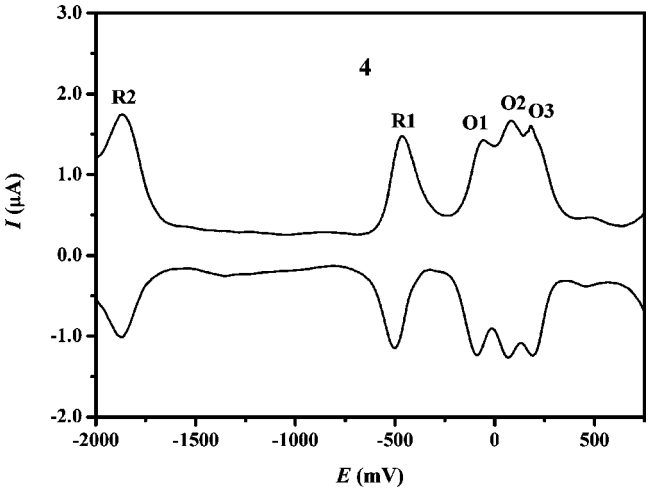

Figure 5. Differential pulse voltammetry of Lu(*Pc*)[Por(Fc)$_2$] (**4**) in CH_2Cl_2 containing 0.1 M [NBu_4][ClO_4] at a scan rate of 10 mV s^{-1}.

for Lu(*Pc*)[Por(Fc)$_2$] (**4**) along with the decrease of rare earth radius, also indicating the increase in the ring-to-ring $\pi-\pi$ interaction in the double-deckers in the same order. As can be seen in Figures 5 and S4 (Supporting Information), the double-decker complexes **1**−**4** display another two consecutive one-electron oxidation waves, the first (O1) and second oxidation (O2) processes, which are clearly due to the ferrocenyl units,[8,13b] indicating the effective electronic coupling between the two ferrocene centers attached at the two opposite *meso*-positions of the porphyrin ligand in the double-decker complexes. By contrast, a single two-electron oxidation attributed to the ferrocenyl groups is observed for their monomeric counterparts MPor(Fc)$_2$ (M = 2H, Ni), Figure S5 (Supporting Information), revealing the lack of electronic coupling between the two porphyrin *meso*-attached ferrocenyl groups due to their free rotation along the C(*meso*)−C(*ipso*) bond, as is proved by the very small rotation energy barrier according to the DFT calculation result described below.

Obviously, sandwich molecular structure plays an important role in adjusting a suitable orientation between the two porphyrin *meso*-attached ferrocene units and inducing effective electronic interaction due to the restricted rotation of ferrocenyl groups along the C(*meso*)−C(*ipso*) bond of Por(Fc)$_2$ associated with the steric hindrance from the *Pc* ring in the mixed (phthalocyaninato)(porphyrinato) rare earth sandwich complexes.[13] As described in the structural studies section and illustrated by the optimized molecular structures (see the DFT calculations section below) along with rare earth contraction, the distance between the Por and *Pc* rings gradually diminishes, while the doming extent of the Por and *Pc* rings as well as the ring-to-ring $\pi-\pi$ interaction increases from **1** to **4**.[14] This in turn results in a gradual increase in the electronic coupling between the two ferrocene centers linked with the sandwich (phthalocyaninato)(porhyrinato) rare earth double-decker framework. As a consequence, the separation between the two ferrocene-based one-electron oxidation processes gradually increases from 81 mV for **1** to 156 mV for **4** along with the rare earth contraction, Figure 6. Nevertheless, as displayed in

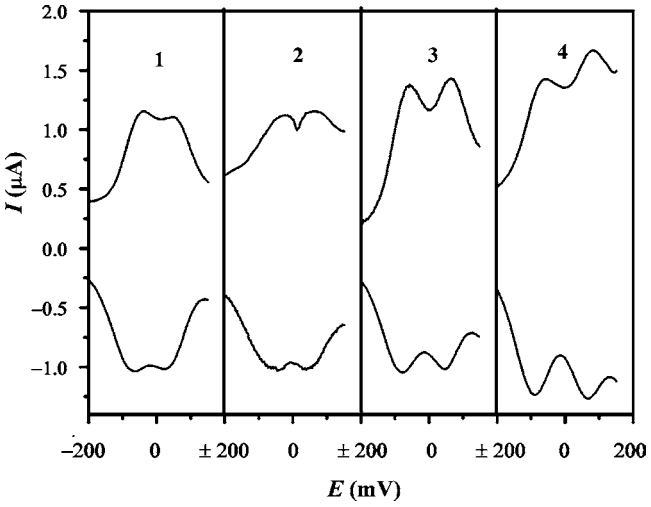

Figure 6. Differential pulse voltammetry of the two ferrocene-based one-electron oxidation processes of double-deckers **1**−**4** in CH_2Cl_2 containing 0.1 M [NBu_4][ClO_4] at a scan rate of 10 mV s^{-1}.

Figure 7, a linear correlation exists between the value of $\Delta E^{\circ\prime}_{1/2}$ = Oxd_1 − Oxd_2 and the rare earth ionic radius,

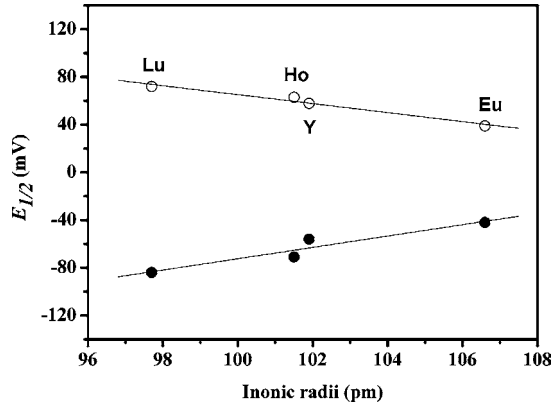

Figure 7. Half-wave potentials of the two ferrocene-based one-electron oxidation processes of M(*Pc*)[Por(Fc)$_2$] [M = Eu (**1**), Y (**2**), Ho (**3**), Lu (**4**)] as a function of the ionic radius of M^{III}.

illustrating that the electronic interaction between the two ferrocene centers linked via sandwich bis(tetarpyrrole) rare

Table 4. Half-Wave Redox Potentials (mV) of Double- and Triple-Deckers 1−5 in CH_2Cl_2 Containing 0.1 M [Bu_4N][ClO_4]

	ferrocene			double/triple-decker					
cmpd	Oxd_1	Oxd_2	$\Delta E^{\circ\prime}_{1/2}$ [a]	Red_3	Red_2	Red_1	Oxd_3	Oxd_4	$\Delta E^{\circ}_{1/2}$ [b]
1	−42	39	81		−1823	−406	305		1417
2	−56	58	114		−1856	−467	265		1389
3	−71	63	134		−1844	−459	245		1385
4	−84	72	156		−1863	−483	204		1380
5	−18	28	46	−2046	−1589	−1208	−103	431	

[a] $\Delta E^{\circ\prime}_{1/2}$ = Oxd_1 − Oxd_2. [b] $\Delta E^{\circ}_{1/2}$ = Red_1 − Red_2.

dx.doi.org/10.1021/ic202613r | *Inorg. Chem.* 2012, 51, 5651−5659

earth framework can be tuned via changing the rare earth ion. The electronic coupling in complexes **1**−**4** (i.e., the separation between the two ferrocene-based one-electron oxidation processes) are much smaller than that of 5,15-bis(ferrocenyl)-β-octaalkyl-porphyrins found by Boyd et al.[8] and Rhee et al,[8b] indicating a smaller separation between the positive and negative combination of orbitals in the present case. The somewhat weaker coupling for complexes **1**−**4** can also be explained by the weak orbital mixing extent of ferrocenyl molecular orbital system with the π system of the porphyrin connector. In addition, the Fe−Fe distance in the single crystal molecular structures of **1** and **4** (13.065 and 13.426 Å) is much longer than that in the crystal structure of 5,15-bis(ferrocenyl)-β-octaalkyl-porphyrins (10.3 and 11.2 Å for nickel and metal-free species, respectively),[8] resulting in the much smaller electronic coupling strength.

It is worth noting that associated with the increased ring-to-ring distance and weakened $\pi-\pi$ interaction in the triple-decker tetrapyrrole rare earth complexes, the two outer tetarpyrrole rings in sandwich tris(tetrapyrrole) rare earth triple-decker complexes become less doming in comparison with those in the bis(tetrapyrrole) rare earth counterparts.[13,14] As a consequence, electronic interaction between the two ferrocene centers can also be tuned through changing the linking sandwich framework from double-decker to triple-decker. This is verified by the electrochemical investigation results on $Eu_2(Pc)_2$[Por-$(Fc)_2$] (**5**), **Figure S7** (Supporting Information) and Table 4. In comparison with Eu(*Pc*)[$Por(Fc)_2$] (**1**), the splitting between the two ferrocene-based one-electron oxidations for triple-decker **5**, 46 mV, becomes smaller than that for its double-decker counterpart **1**, 81 mV.

DFT Calculations. To further understanding the electronic coupling between ferrocenyl groups, DFT calculations on $H_2Por(Fc)_2$ and the reduced species of **2** and La(*Pc*)[$Por(Fc)_2$] are carried out.[17] According to the calculation result, the isomer of $H_2Por(Fc)_2$ with the two Fc groups on the two different sides of the mean porphyrin plane, $H_2Por(trans\text{-}Fc)_2$, is a little more stable than that on the same side, $H_2Por(syn\text{-}Fc)_2$. However, because of the very small energy difference between $H_2Por(trans\text{-}Fc)_2$ and $H_2Por(syn\text{-}Fc)_2$, only 0.53 kcal/mol, neither of the two isomers can be dominant over the other thermodynamically. In fact, the rotation barrier of one Fc group along the C(*meso*)−C(*ipso*) bond calculated in a tight potential energy surface scan is only 4.64 kcal/mol, indicating the almost free rotation of Fc groups in $H_2Por(Fc)_2$. This corresponds well with the electrochemical result that only a single two-electron oxidation attributed to the ferrocenyl groups instead of two one-electron oxidation is observed for the monomeric compounds $MPor(Fc)_2$ (M = 2H, Ni).

Figure S6 (Supporting Information) shows the optimized molecular structure of the reduced species of **2** and La(*Pc*)[$Por(Fc)_2$]. The optimized molecular structures for both species have C_2 symmetry, which ensures the two Fc groups in each species are treated equivalently. As can be seen, in the energy-minimized molecular structure of $\{Y(Pc)[Por(Fc)_2]\}^-$ ($\mathbf{2}^-$) and $\{La(Pc)[Por(Fc)_2]\}^-$, the two porphyrin *meso*-attached ferrocenyl units adopt a *syn*-configuration with respect to the porphyrin ring. The probable reason is that the $\pi-\pi$ interaction between Por and *Pc* rings in the double-decker complexes hinders the free rotation of Fc groups and makes the the *syn*-configuration with two Fc groups lying between the mean Por and *Pc* planes and the *trans*-configuration less stable in energy. In addition, in line with the experimental structure, along with rare earth contraction from La to Y, the distance between the Por and *Pc* rings gradually diminishes from 3.26 to 2.88 Å, while the doming extent of the Por and *Pc* rings increases as demonstrated by the increased dihedral angle of the individual isoindole rings with respect to the corresponding N4 mean plane, from 6.3 and 11.5° for $\{La(Pc)[Por(Fc)_2]\}^-$ to 8.5 and 12.4° for $\{Y(Pc)[Por(Fc)_2]\}^-$. As a result, the calculated Fe−Fe distance decreases from 12.94 Å in $\{La(Pc)[Por(Fc)_2]\}^-$ to 12.78 Å in $\{Y(Pc)[Por(Fc)_2]\}^-$, resulting in the much smaller electronic coupling term V_{ab} according to Hush formula.[18]

Figure 8 shows the molecular orbital energy level and orbital symmetry of La$\{(Pc)[Por(Fc)_2]\}^-$ and $\{Y(Pc)[Por(Fc)_2]\}^-$ as well as the orbital maps of $\{Y(Pc)[Por(Fc)_2]\}^-$ for orbitals from HOMO − 9 to LUMO + 5. As can be seen, the HOMO,

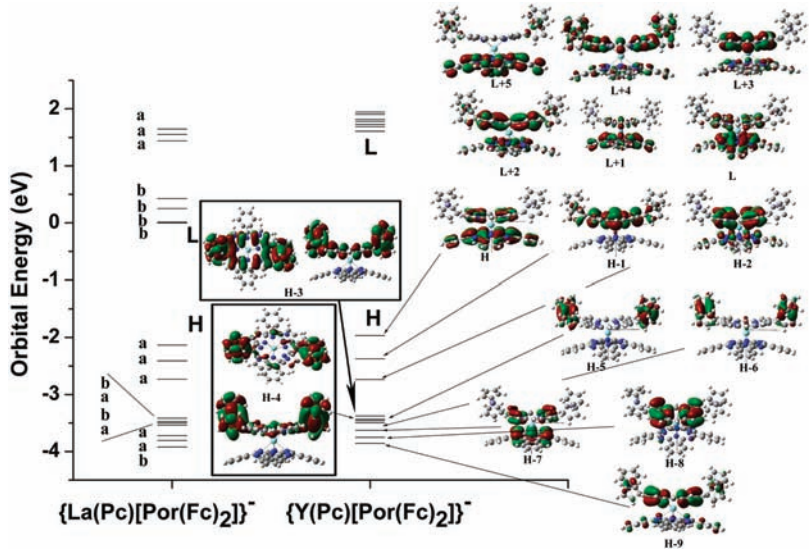

Figure 8. Molecular orbital energy level and orbital symmetry of La$\{(Pc)[Por(Fc)_2]\}^-$ and $\{Y(Pc)[Por(Fc)_2]\}^-$ as well as the orbital maps of $\{Y(Pc)[Por(Fc)_2]\}^-$ for orbitals from HOMO − 9 to LUMO + 5. The map of orbitals for La$\{(Pc)[Por(Fc)_2]\}^-$ are very similar to those of $\{Y(Pc)[Por(Fc)_2]\}^-$ and therefore are not shown. Orbital maps for HOMO − 3 and HOMO − 4 were obtained with the isovalue of 0.008, while others were obtained with the isovalue of 0.02.

dx.doi.org/10.1021/ic202613r | *Inorg. Chem.* 2012, 51, 5651−5659

HOMO − 1, and HOMO − 2 orbitals of $\{Y(Pc)[Por(Fc)_2]\}^-$ are typical orbitals of mixed (porphyrinato)(phthalocyaninato) rare earth double-decker complexes with some small contribution from the Fe atoms of Fc groups in HOMO − 1 orbital.[17b] The HOMO − 3 in this system is mainly composed of ferrocene Fe *d* orbitals of both ferrocene groups and π orbital of porphyrin ligand in the (phthalocyaninato)(porphyrinato) rare earth double-decker complexes with some contribution from the cyclopentadiene groups of ferrocene. The HOMO − 4 orbital has the same characteristic as the HOMO − 3 orbital, but the sign of some orbital nodes reverses, and the orbital distribution on porphyrin ligand decreases a little. The HOMO − 3 and HOMO − 4 molecular orbitals thus correspond to the negative and positive combination of orbitals composed of both ferrocenes and porphyrin. It has been proposed that the strength of the electronic coupling between ferrocene centers in multicomponent systems is related to the separation between the positive and negative combination of orbitals composed of both ferrocenes and connectors.[8] The calculated electronic coupling according to the orbital difference between HOMO − 3 and HOMO − 4 orbitals in the monoanion of **2** is about 0.060 eV, which is slightly larger than that in the monoanion of $La(Pc)[Por(Fc)_2]$ with the value of 0.059 eV. These results are in line with the experimental results that the separation between the two ferrocene-based one-electron oxidation processes increases along with the rare earth contraction. At the end of this section, it is worth noting that the calculated orbital energy and orbital maps are based on the reduced species $La\{(Pc)[Por(Fc)_2]\}^-$ and $\{Y(Pc)[Por(Fc)_2]\}^-$, thus oxidization of these reduced species will first occur on *Pc* and Por macrocycles. In addition, the limitation of the DFT calculation may also underestimate the orbital energy of the ferrocene fragment. As a result, the HOMO, HOMO − 1, and HOMO − 2 orbitals of the reduced species $La\{(Pc)[Por(Fc)_2]\}^-$ and $\{Y(Pc)[Por(Fc)_2]\}^-$ do not correspond to the experimentally observed first and second oxidation.

CONCLUSIONS

In conclusion, a new method has been developed to induce electronic interaction between remote redox-active centers. Two ferrocene units linked with sandwich (phthalocyaninao)(porphyrinato) rare earth complex framework exhibit effective electronic coupling. In particular, such an electronic interaction can be easily tuned through changing either the rare earth metal or the sandwich form from double- to triple-decker. This provides a new pathway for constructing novel molecular systems containing multiple photo- and redox-active centers with long-range electronic interaction for potential applications in molecular electronics.

EXPERIMENTAL SECTION

General Remarks. Dichloromethane and 1,2,4-trichlorobenzene (TCB) were distilled from CaH_2 under nitrogen. *n*-Octanol was distilled from sodium under nitrogen. Column chromatography was carried out on silica gel (Merck, Kieselgel 60, 70-230 mesh) and biobeads (BIORAD S-X1, 200-400 mesh) columns with the indicated eluents. All other reagents and solvents were used as received. The compounds $M(acac)_3{\cdot}nH_2O$ (M = Eu, Y, Ho, Lu),[19] $Eu(Pc)_2$,[20] dipyrrylmethane,[21] and ferrocene aldehyde[22] were prepared according to the published procedures. $H_2Por(Fc)_2$ and $NiPor(Fc)_2$ were prepared according to the published methods;[15] for details, see the Supporting Information.

^1H NMR spectra were recorded on a Bruker DPX 300 spectrometer (300 MHz). Spectra were referenced internally using the residual solvent resonances relative to $SiMe_4$. Electronic absorption spectra were recorded on a Hitachi U-4100 spectrophotometer. MALDI-TOF mass spectra were taken on a Bruker BIFLEX III ultrahigh resolution Fourier transform ion cyclotron resonance (FT-ICR) mass spectrometer with α-cyano-4-hydroxycinnamic acid as the matrix. Elemental analyses were performed by the Institute of Chemistry, Chinese Academy of Sciences. Electrochemical measurements were carried out with a BAS CV-50W voltammetric analyzer. The cell comprised inlets for a glassy carbon disk working electrode of 2.0 mm in diameter and a silver-wire counter electrode. The reference electrode was Ag/Ag^+, which was connected to the solution by a Luggin capillary whose tip was placed close to the working electrode. It was corrected for junction potentials by being referenced ex- or internally to the ferrocenium/ferrocene (Fc^+/Fc) couple [$E_{1/2}(Fc^+/Fc)$ = 501 mV vs SCE]. Typically, a 0.1 mol dm^{-3} solution of $[Bu_4N][ClO_4]$ in CH_2Cl_2 containing 0.5 mmol dm^{-3} of sample was purged with nitrogen for 10 min, then the voltammograms were recorded at ambient temperature. The scan rate was 20 and 10 mV s^{-1} for CV and DPV, respectively.

General Procedure for the Preparation of M(*Pc*)[Por(Fc)$_2$] (M = Eu, Y, Ho, Lu) (1−4). A mixture of $M(acac)_3{\cdot}nH_2O$ (0.1 mmol), phthalonitrile (0.6 mmol), and DBU (40 mg, 0.26 mmol) in *n*-octanol (5 mL) was stirred at 120 °C for 2 h under nitrogen. After being cooled to room temperature, $H_2Por(Fc)_2$ (34 mg, 0.05 mol) was added and the resulting mixture was heated to reflux for 7.5 h. After removing the volatiles under reduced pressure, the residue was chromatographed on a silica gel column with $CHCl_3$ as the eluent. A small amount of unreacted metal free $H_2Por(Fc)_2$ was eluted first. Then, a brown band containing the target double-decker compound was developed. Repeated chromatography followed by recrystallization from $CHCl_3$ and MeOH gave pure target compounds as brown crystals in the yields of 5−20%.

Preparation of Eu$_2$(*Pc*)$_2$[Por(Fc)$_2$] (5). A mixture of $Eu(acac)_3{\cdot}nH_2O$ (15 mg, 0.03 mmol), $H_2Por(Fc)_2$ (14 mg, 0.02 mmol), and $Eu(Pc)_2$ (23 mg, 0.02 mmol) in TCB (4 mL) was heated to reflux for 3 h under nitrogen. The resulting dark-blue solution was cooled to room temperature, the volatiles were removed under reduced pressure. The residue was chromatographed on a silica gel column with $CHCl_3$ as the eluent. The first blue band containing triple-decker compound $Eu_2(Pc)_2[Por(Fc)_2]$ was eluted. Repeated chromatography on a biobeads column followed by recrystallization from $CHCl_3$ and

Table 5. Crystallographic Data for 1 and 4

	1·$CHCl_3$	**4**·$CHCl_3{\cdot}CH_3CH_2OH$
molecular formula	$C_{73}H_{45}Cl_3EuFe_2N_{12}$	$C_{75}H_{51}Cl_3EuFe_2N_{12}O$
M	1460.22	1529.25
crystal system	triclinic	monoclinic
space group	$P\bar{1}$	$P2/c$
a (Å)	14.0455(9)	19.4185(3)
b (Å)	14.6373(8)	18.8442(3)
c (Å)	16.2622(9)	17.3971(2)
α (deg)	104.895(5)	90
β (deg)	93.267(5)	101.4450(10)
γ (deg)	116.198(6)	90
V (Å^3)	2842.5(3)	6239.47(16)
Z	2	4
F(000)	1466	3132
D_c/Mg m^{-3}	1.706	1.668
data collection range (deg)	2.87 to 60.00	3.30 to 60.00
reflections collected	16 907	18 929
independent reflections	8374	9206
R_1 [$I > 2\sigma(I)$]	0.0514	0.0707
wR_2 [$I > 2\sigma(I)$]	0.1241	0.2081
R_1 [for all]	0.0643	0.0848
wR_2 [for all]	0.1340	0.2184
goodness of fit	1.019	1.059

dx.doi.org/10.1021/ic202613r | *Inorg. Chem.* 2012, 51, 5651−5659

MeOH gave pure target compound as black needle-like crystals (29 mg, 70%).

X-ray Crystallographic Analyses. Crystal data and details of data collection and structure refinement are given in Table 5. The crystallographical data of **1** and **4** were determined by X-ray diffraction analysis at 120 K using Oxford Diffraction Gemini E system with $Cu_{K\alpha}$ radiation λ = 1.5418 Å. The structures were solved by the direct method (SHELXS-97) and refined by full-matrix least-squares (SHELXL-97) on F^2.[23] Anisotropic thermal parameters were used for the nonhydrogen atoms and isotropic parameters for the hydrogen atoms. Hydrogen atoms were added geometrically and refined using a riding model. CCDC-856389 and 856390 contain the supplementary crystallographic data for this paper. These data can be obtained free of charge from the Cambridge Crystallographic Data Centre via www.ccdc.cam.ac.uk/data_request/cif.

Computational Details. The hybrid density functional B3LYP (Becke−Lee−Yang−Parr composite of the exchange-correlation functional) method[24] and the basis sets with LANL2DZ[25] for the Y and La atoms and 6-31G*(d) for all other atoms were used. The C_2 symmetry in the input geometry was detected and kept during geometry optimization process. All calculations were carried out using the Gaussian 03 program[26] in the IBM P690 system at the Shandong Province High Performance Computing Centre.

■ ASSOCIATED CONTENT

Ⓢ Supporting Information

Synthesis of $H_2Por(Fc)_2$ and $NiPor(Fc)_2$; ^1H NMR spectrum of $Lu(Pc)[Por(Fc)_2]$ (**4**); $^1H-^1H$ COSY spectrum of $Lu(Pc)[Por(Fc)_2]$ (**4**); molecular structure of $Lu(Pc)[Por(Fc)_2]$ (**4**); cyclic voltammetry of **1**−**4** in CH_2Cl_2; cyclic voltammetry of $H_2Por(Fc)_2$ and $Ni[Por(Fc)_2]$ in CH_2Cl_2; optimized molecular structures of $La(Pc)[Por(Fc)_2]^-$ and $Y(Pc)[Por(Fc)_2]^-$ at the B3LYP/6-31G*/LANL2DZ level; differential pulse voltammetry and cyclic voltammetry of $Eu_2(Pc)_2[Por(Fc)_2]$ (**5**) in CH_2Cl_2; ^1H NMR data (δ ppm) for **1**, **2**, **4**, and **5**; complete ref 26; and crystallographic data of **1** and **4** (CIF). This material is available free of charge via the Internet at http://pubs.acs.org.

■ AUTHOR INFORMATION

Corresponding Author

*E-mail: yzbian@ustb.edu.cn (Y.B.); jianzhuang@ustb.edu.cn (J.J.).

Notes

The authors declare no competing financial interest.

■ ACKNOWLEDGMENTS

Financial support from the Natural Science Foundation of China, Ministry of Education of China, the Postdoctoral Scientific Foundation of Shandong (Grant no. 200903058), and the Doctoral Foundation of Shandong (Grant no. 2007BS02016) is gratefully acknowledged.

■ REFERENCES

(1) Fox, M. A. *Acc. Chem. Res.* **1999**, *32*, 201−207.

(2) Joachim, C.; Gimzewski, J. K.; Aviram, A. *Nature* **2000**, *408*, 541−548.

(3) (a) Barlow, S.; O'Hare, D. *Chem. Rev.* **1997**, *97*, 637−670. (b) Ceccon, A.; Santi, S.; Orian, L.; Bisello, A. *Coord. Chem. Rev.* **2004**, *248*, 683−724. (c) Aguirre-Etcheverry, P.; O'Hare, D. *Chem. Rev.* **2010**, *110*, 4839−4864.

(4) (a) Kadish, K. M., Smith, K. M., Guilard, R., Eds. *The Porphyrin Handbook*; Academic Press: San Diego, CA, 2000−2003; Vols. *1*−*10*, *11*−*20*. (b) Kadish, K. M., Smith, K. M., Guilard, R., Eds. *Handbook of Porphyrin Science: With Applications to Chemistry, Physics, Materials Science, Engineering, Biology and Medicine*; World Scientific: Singapore, 2010−2011; Vols. *1*−*10*, *11*−*15*.

(5) (a) Leznoff, C. C., Lever, A. B. P., Eds. *Phthalocyanines: Properties and Applications*; VCH Publishers: New York, 1989−1996; Vols. *1*−*4*. (b) Jiang, J. Advances in Functional Phthalocyanine Materials. In *Structure and Bonding*; Mingos, D. M. P., Ed.; Springer-Verlag: Heidelberg, Germany, 2010; Vol. *135*.

(6) For systems containing multiferroceynl units linked with porphyrin, see, for example: (a) Wollmann, R. G.; Hendrickson, D. N. *Inorg. Chem.* **1977**, *16*, 3079−3089. (b) Schmidt, E. S.; Calderwood, T. S.; Bruice, T. C. *Inorg. Chem.* **1986**, *25*, 3718−3720. (c) Kadish, K. M.; Xue, Q. Y.; Barbe, J.-M. *Inorg. Chem.* **1987**, *26*, 2565−2566. (d) Beer, P. D.; Drew, M. G. B.; Hesek, D.; Jagessar, R. *Chem. Commun.* **1995**, 1187−1189. (e) Hodgson, M. C.; Burrell, A. K.; Boyd, P. D. W.; Brothers, P. J.; Rickard, C. E. F. *J. Porphyrins Phthalocyanines* **2002**, *6*, 737−747. (f) Suijkerbuijk, B. M. J. M.; Gebbink, R. J. M. K. *Angew. Chem., Int. Ed.* **2008**, *47*, 7396−7421. (g) Bucher, C.; Devillers, C. H.; Moutet, J. C.; Royal, G.; Saint-Aman, E. *Coord. Chem. Rev.* **2009**, *253*, 21−36. (h) Solntsev, P. V.; Sabin, J. R.; Dammer, S. J.; Gerasimchuk, N. N.; Nemykin, V. N. *Chem. Commun.* **2010**, *46*, 6581−6583. (i) Gryko, D. T.; Zhao, F.; Yasseri, A. A.; Roth, K. M.; Bocian, D. F.; Kuhr, W. G.; Lindsey, J. S. *J. Org. Chem.* **2000**, *65*, 7356−7362. (j) Beer, P. D.; Drew, M. G. B.; Jagessar, R. *Dalton Trans.* **1997**, 881−886.

(7) For systems containing multiferroceynl units linked with phthalocyanine, see, for example: (a) Jin, Z.; Nolan, K.; McArthur, C. R.; Lever, A. B. P.; Leznoff, C. C. *J. Organomet. Chem.* **1994**, *468*, 205−212. (b) Dabak, S.; Bekaroglu, Ö. *New J. Chem.* **1997**, *21*, 267−271. (c) Silver, J.; Sosa-Sanchez, J. L.; Frampton, C. S. *Inorg. Chem.* **1998**, *37*, 411−417. (d) Poon, K.-W.; Yan, Y.; Li, X.; Ng, D. K. P. *Organometallics* **1999**, *18*, 3528−3533. (e) Poon, K.-W.; Liu, W.; Chan, P.-K.; Yang, Q.; Chan, T.-W. D.; Mak, T. C. W.; Ng, D. K. P. *J. Org. Chem.* **2001**, *66*, 1553−1559. (g) Nemykin, V. N.; Kobayashi, N. *Chem. Commun.* **2001**, 165−166. (h) Çamur, M.; Esenpınar, A. A.; Özkaya, A. R.; Bulut, M. *J. Organomet. Chem.* **2011**, *696*, 1868−1873. (i) Sun, L.; Wang, S.; Tian, H. *Chem. Lett.* **2007**, *36*, 250−251.

(8) Boyd, P. D. W.; Burrell, A. K.; Campbell, W. M.; Cocks, P. A.; Gordon, K. C.; Jameson, G. B.; Officer, D. L.; Zhao, Z. *Chem. Commun.* **1999**, 637−638. (b) Rhee, S. W.; Na, Y. H.; Do, Y.; Kim, J. *Inorg. Chim. Acta* **2000**, *309*, 49−56. (c) Auger, A.; Muller, A. J.; Swarts, J. C. *Dalton Trans.* **2007**, *33*, 3623−3633. (d) Auger, A.; Swarts, J. C. *Organometallics* **2007**, *26*, 102−109. (e) Loim, N. M.; Abramova, N. V.; Sokolov, V. I. *Mendeleev Commun.* **1996**, *6*, 46−47. (f) Nemykin, V. N.; Barrett, C. D.; Hadt, R. G.; Subbotin, R. I.; Maximov, A. Y.; Polshin, E. V.; Koposov, A. Y. *Dalton Trans.* **2007**, 3378−3389. (g) Nemykin, V. N.; Pierluca Galloni, P.; Floris, B.; Barrett, C. D.; Hadt, R. G.; Subbotin, R. I.; Marrani, A. G.; Zanoni, R.; Loim, N. M. *Dalton Trans.* **2008**, 4233−4246. (h) Nemykin, V. N.; Rohde, G. T.; Barrett, C. D.; Hadt, R. G.; Bizzarri, C.; Galloni, P.; Floris, B.; Nowik, I.; Herber, R. H.; Marrani, A. G.; Zanoni, R.; Loim, N. M. *J. Am. Chem. Soc.* **2009**, *131*, 14969−14978. (i) Nemykin, V. N.; Rohde, G. T.; Barrett, C. D.; Hadt, R. G.; Sabin, J. R.; Reina, G.; Galloni, P.; Floris, B. *Inorg. Chem.* **2010**, *49*, 7497−7509. (j) Rohde, G. T.; Sabin, J. R.; Barrett, C. D.; Nemykin, V. N. *New J. Chem.* **2011**, *35*, 1440−1448.

(9) (a) Jiang, J.; Ng, D. K. P. *Acc. Chem. Res.* **2009**, *42*, 79−88. (b) Bian, Y.; Zhang, Y.; Ou, Z.; Jiang, J. In *Handbook of Porphyrin Science: With Applications to Chemistry, Physics, Materials Science, Engineering, Biology and Medicine*; Kadish, K. M., Smith, K. M., Guilard, R., Eds.; World Scientific: Singapore, 2011; Vol. *14*, Chapter 64, pp 249−460.

(10) (a) Chen, Y.; Su, W.; Bai, M.; Jiang, J.; Li, X.; Liu, Y.; Wang, L.; Wang, S. *J. Am. Chem. Soc.* **2005**, *127*, 15700−15701. (b) Li, R.; Ma, P.; Dong, S.; Zhang, X.; Chen, Y.; Li, X.; Jiang, J. *Inorg. Chem.* **2007**, *46*, 11397−11404. (c) Chen, Y.; Li, R.; Wang, R.; Ma, P.; Dong, S.; Gao, Y.; Li, X.; Jiang, J. *Langmuir* **2007**, *23*, 12549−12554. (d) Su, W.; Jiang, J.; Xiao, K.; Chen, Y.; Zhao, Q.; Yu, G.; Liu, Y. *Langmuir* **2005**, *21*, 6527−6531.

(11) (a) Ishikawa, N.; Sugita, M.; Ishikawa, T.; Koshihara, S.; Kaizu, Y. *J. Phys. Chem. B* **2004**, *108*, 11265−11271. (b) Ishikawa, N.; Sugita, M.; Wernsdorfer, W. *Angew. Chem., Int. Ed.* **2005**, *44*, 2931−2935.

(12) Liu, Z.; Yasseri, A. A.; Lindsey, J. S.; Bocian, D. F. *Science* **2003**, *302*, 1543−1545.
(13) (a) Sun, X.; Li, R.; Wang, D.; Dou, J.; Zhu, P.; Lu, F.; Ma, C.; Ng, D. K. P.; Kobayashi, N.; Jiang, J. *Eur. J. Inorg. Chem.* **2004**, 3806−3813. (b) Lu, F.; Sun, X.; Li, R.; Liang, D.; Zhu, P.; Zhang, X.; Choi, C.-F.; Ng, D. K. P.; Fukuda, T.; Kobayashi, N.; Jiang, J. *New J. Chem.* **2004**, *28*, 1116−1122.
(14) (a) Jiang, J.; Bian, Y.; Furuya, F.; Liu, W.; Choi, M. T. M.; Kobayashi, N.; Li, H.-W.; Yang, Q.; Mak, T. C. W.; Ng, D. K. P. *Chem.—Eur. J.* **2001**, *7*, 5059−5069. (b) Bian, Y.; Wang, D.; Wang, R.; Weng, L.; Dou, J.; Zhao, D.; Ng, D. K. P.; Jiang, J. *New J. Chem.* **2003**, *27*, 844−849. (c) Bian, Y.; Jiang, J.; Tao, Y.; Choi, M. T. M.; Li, R.; Ng, A. C. H.; Zhu, P.; Pan, N.; Sun, X.; Arnold, D. P.; Zhou, Z.; Li, H.-W.; Mak, T. C. W.; Ng, D. K. P. *J. Am. Chem. Soc.* **2003**, *125*, 12257−12267.
(15) (a) Lee, C.-H.; Lindsey, J. S. *Tetrahedron* **1994**, *50*, 11427−11440. (b) Lindsey, J. S. In *The Porphyrin Handbook*; Kadish, K. M., Smith, K. M., Guilard, R., Eds.; Academic Press: San Diego, CA, 2000; Vol. *1*, pp 45−118.
(16) (a) Arnold, D. P.; Jiang, J. *J. Phys. Chem. A* **2001**, *105*, 7525−7533. (b) Birin, K. P.; Gorbunova, Y. G.; Tsivadze, A. Y. *Magn. Reson. Chem.* **2010**, *48*, 505−515.
(17) (a) Zhang, L.; Qi, D.; Zhang, Y.; Bian, Y.; Jiang, J. *J. Mol. Graphics Modell.* **2011**, *29*, 717−725. (b) Zhang, Y.; Cai, X.; Yao, P.; Xu, H.; Bian, Y.; Jiang, J. *Chem.—Eur. J.* **2007**, *13*, 9503−9514.
(18) Hush, N. S. *Coord. Chem. Rev.* **1985**, *64*, 135−157.
(19) Stites, J. G.; McCarty, C. N.; Quill, L. L. *J. Am. Chem. Soc.* **1948**, *70*, 3142−3143.
(20) Liu, W.; Jiang, J.; Du, D.; Arnold, D. P. *Aust. J. Chem.* **2000**, *53*, 131−136.
(21) Littler, B. J.; Miller, M. A.; Hung, C. H.; Wagner, R. W.; Lindsey, J. S. *J. Org. Chem.* **1999**, *64*, 1391−1396.
(22) Sato, M.; Kono, H.; Shiga, M.; Motoyama, I.; Hata, K. *Bull. Chem. Soc. Jpn.* **1968**, *41*, 252−252.
(23) *SHELXL Reference Manual*, version 5.1; Bruker Analytical X-Ray Systems: Madison, WI, 1997.
(24) (a) Lee, C.; Yang, W.; Parr, R. G. *Phys. Rev. B* **1988**, *37*, 785−789. (b) Becke, A. D. *J. Chem. Phys.* **1993**, *98*, 5648−5652.
(25) (a) Hay, P. J.; Wadt, W. R. *J. Chem. Phys.* **1985**, *82*, 299−310. (b) Dunning, T. H.; Hay, P. J. In *Modern Theoretical Chemistry*; Schaefer, H. F., III., Ed.; Plenum: New York, 1976; Vol. *3*.
(26) Frisch, M. J., et al. *Gaussian 03*, revision B.05; Gaussian, Inc.: Wallingford, CT, 2004.